



# CHORUS

This is the accepted manuscript made available via CHORUS. The article has been published as:

## Nature of low-lying electric dipole resonance excitations in $^{74}\text{Ge}$

D. Negi *et al.*

Phys. Rev. C **94**, 024332 — Published 23 August 2016

DOI: [10.1103/PhysRevC.94.024332](https://doi.org/10.1103/PhysRevC.94.024332)

# Nature of low-lying electric dipole resonance excitations in $^{74}\text{Ge}$

D. Negi,<sup>1,2,\*</sup> M. Wiedeking,<sup>1,†</sup> E. G. Lanza,<sup>3</sup> E. Litvinova,<sup>4,5</sup> A. Vitturi,<sup>6,7</sup> R. A. Bark,<sup>1</sup>  
L. A. Bernstein,<sup>8,9</sup> D. L. Bleuel,<sup>8</sup> S. Bvumbi,<sup>10</sup> T. D. Bucher,<sup>1</sup> B. H. Daub,<sup>8,9</sup> T. S. Dinoko,<sup>1,11</sup>  
J. L. Easton,<sup>1,11</sup> A. Gørgen,<sup>12</sup> M. Guttormsen,<sup>12</sup> P. Jones,<sup>1</sup> B. V. Kheswa,<sup>1,13</sup> N. A. Khumalo,<sup>11,14</sup>  
A. C. Larsen,<sup>12</sup> E. A. Lawrie,<sup>1</sup> J. J. Lawrie,<sup>1</sup> S. N. T. Majola,<sup>1,15</sup> L. P. Masiteng,<sup>10</sup> M. R. Nchodu,<sup>1</sup>  
J. Ndayishimye,<sup>1,13</sup> R. T. Newman,<sup>13</sup> S. P. Noncolela,<sup>1,11</sup> J. N. Orce,<sup>11</sup> P. Papka,<sup>1,13</sup>  
L. Pellegrini,<sup>1,16</sup> T. Renstrøm,<sup>12</sup> D. G. Roux,<sup>17</sup> R. Schwengner,<sup>18</sup> O. Shirinda,<sup>1</sup> and S. Siem<sup>12</sup>

<sup>1</sup>*iThemba LABS, P.O. Box 722, Somerset West 7129, South Africa*

<sup>2</sup>*Centre for Excellence in Basic Sciences, Vidyagari Campus, Mumbai 400098, India*

<sup>3</sup>*INFN, Sezione di Catania, I-95123 Catania, Italy*

<sup>4</sup>*Western Michigan University, Kalamazoo, MI 49008-5252, USA*

<sup>5</sup>*National Superconducting Cyclotron Laboratory, Michigan State University, East Lansing, Michigan 48824-1321, USA*

<sup>6</sup>*Dipartimento di Fisica e Astronomia, Università di Padova, Italy*

<sup>7</sup>*INFN, Sezione di Padova, I-35131 Padova, Italy*

<sup>8</sup>*Lawrence Livermore National Laboratory, Livermore, CA 94550-9234, USA*

<sup>9</sup>*University of California, Berkeley, CA 94720-1730, USA*

<sup>10</sup>*University of Johannesburg, Auckland Park 2006, South Africa*

<sup>11</sup>*University of the Western Cape, Bellville 7535, South Africa*

<sup>12</sup>*University of Oslo, N-0316 Oslo, Norway*

<sup>13</sup>*Stellenbosch University, Matieland 7602, South Africa*

<sup>14</sup>*University of Zululand, KwaDlangezwa 3886, South Africa*

<sup>15</sup>*University of Cape Town, Rondebosch 7701, South Africa*

<sup>16</sup>*University of the Witwatersrand, Johannesburg 2050, South Africa*

<sup>17</sup>*Rhodes University, Grahamstown 6410, South Africa*

<sup>18</sup>*Helmholtz-Zentrum Dresden-Rossendorf, 01328 Dresden, Germany*

Isospin properties of dipole excitations in  $^{74}\text{Ge}$  are investigated using the  $(\alpha, \alpha'\gamma)$  reaction and compared to  $(\gamma, \gamma')$  data. The results indicate that the dipole excitations in the energy region of 6 to 9 MeV adhere to the scenario of the recently found splitting of the region of dipole excitations into two separated parts: one at low energy being populated by both isoscalar and isovector probes and the other at high energy, excited only by the electromagnetic probe. RQTBA calculations show a reduction in the isoscalar  $E1$  strength with an increase in excitation energy which is consistent with the measurement.

PACS numbers: 21.10.Re, 24.30.Gd, 25.55.Ci, 27.50.+e

## I. INTRODUCTION

In recent years there has been a surge in experimental studies of dipole excitations lying on the low-energy tail of the isovector giant dipole resonance, the so-called Pygmy dipole resonance (PDR). The PDR has been interpreted as an exotic mode of excitation due to the motion of a weakly bound neutron excess against an almost inert proton-neutron core [1–3], although single particle-hole excitations are also considered [4, 5]. One major reason for the renewed interest in the PDR is the possibility of carrying out high-resolution measurements on these low-lying dipole excitations using heavy ion [6, 7], proton [8, 9], and  $\alpha$  inelastic scattering experiments [10, 11]. An experimental technique, combining particle and  $\gamma$ -ray detection techniques, to study the response of dipole excitations to isoscalar probes was pioneered by Poelhekkens *et al.* [12] and applied in several studies since

[6, 7, 10, 11, 13–17]. These experiments provide complementary information to those obtained from  $(\gamma, \gamma')$  experiments which investigate the isovector nature of the excitations [18–24]. One of the surprising results from recent experiments is the isospin splitting of the PDR [2, 3, 10, 11, 13]. This provides intimate knowledge about the isospin nature of these excitations which would not be possible to infer from  $(\gamma, \gamma')$  experiments alone. These experimental discoveries were followed by intensive theoretical investigations [25–30].

Incidentally, scattering experiments with isoscalar probes for the study of the PDR have so far been limited to only certain regions of the nuclear chart and carried out mainly on nuclei with large neutron-to-proton ratios [6, 10, 13, 14, 17]. Information on how the results from scattering reactions compare to those of  $(\gamma, \gamma')$  experiments in nuclei closer to  $N/Z = 1$  are also becoming available [7, 12, 15, 16]. Since most of the incident isoscalar probes are sensitive to the surface of the nucleus, the information gathered advances our understanding of the evolution of the PDR with changing  $N/Z$ . This information is extrapolated for obtaining better estimates of the total strength exhausted by the PDR in nuclei of astro-

\* dinphysics@gmail.com

† wiedeking@tlabs.ac.za

physical importance, many of which are still inaccessible with the available experimental facilities and techniques. The PDR has been suggested to have a significant impact on neutron capture rates and isotopic solar abundance distributions in r-process nucleosynthesis [31–34]. Further, the PDR could possibly constrain the equation-of-state of hot and dense neutron matter as found in neutron star remnants [35, 36].

In this contribution, we present results on  $^{74}\text{Ge}$  where a high-resolution measurement was carried out using the  $\alpha$  inelastic scattering reaction. In its ground state,  $^{74}\text{Ge}$  is a moderately deformed prolate nucleus [37, 38] with  $N/Z = 1.32$ . For comparison and to facilitate the discussion, information about the  $E1$  strength distribution is also available from  $(\gamma, \gamma')$  data in  $^{74}\text{Ge}$  [39, 40].

## II. EXPERIMENTAL DETAILS

The experiment was performed at the Separated Sector Cyclotron facility at iThemba LABS with the AFRODITE  $\gamma$ -ray detector array [41] in conjunction with two identical particle-telescopes, each of them consisting of two silicon detectors (in  $\Delta E - E$  configuration). The  $\alpha$ -particles with a beam energy of 48 MeV impinged on a  $500 \mu\text{g}/\text{cm}^2$  thick  $^{74}\text{Ge}$  target to populate excited states in the inelastic scattering reaction. The experiment was carried out over a period of five days with an average beam current of  $\sim 14$  particle nA. The telescopes were placed at an angle of  $\theta = \pm 45^\circ$  with respect to the beam axis. The dimensions of the W1-type double sided silicon strip detectors [42] were  $5 \text{ cm} \times 5 \text{ cm}$  and consisted of 16 parallel and perpendicular strips 3 mm wide. The distance from target to the telescopes was 5 cm yielding an angular range of  $20^\circ$  to  $72^\circ$  in the laboratory frame of reference. Thicknesses of the  $\Delta E$  and  $E$  detectors were 284 and  $1000 \mu\text{m}$ , respectively, and to suppress  $\delta$  electrons an aluminum foil of  $4.1 \text{ mg}/\text{cm}^2$  areal density was placed in front of the  $\Delta E$  detectors. Calibration of individual strips of the silicon detectors was performed using a  $^{228}\text{Th}$   $\alpha$  source.

AFRODITE, at the time of the experiment, consisted of nine Clover HPGe detectors with four detectors at  $135^\circ$  and five at  $90^\circ$  at a distance of 19.6 cm from the target. The detectors were calibrated using standard  $^{152}\text{Eu}$  and  $^{56}\text{Co}$  sources. High  $\gamma$ -ray energy efficiency parameters for the AFRODITE array were available from Ref. [41]. XIA digital electronics [43] was used to acquire timestamped online data in singles mode.

## III. DATA ANALYSIS

From the timestamped data, events with single, double, and higher fold coincidences were constructed with an offline coincidence time window of 600 ns. From double fold events, the  $\alpha - \gamma$  coincidences were extracted by placing a gate on the  $\alpha$ -particles in the particle identifi-

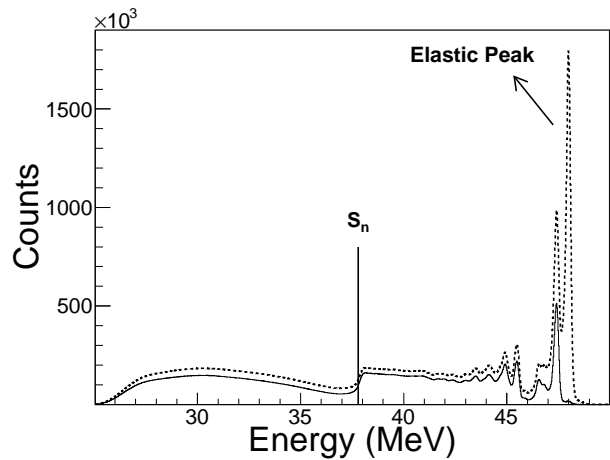


FIG. 1. Spectrum of  $\alpha$  particles detected in coincidence with  $\gamma$ -rays. Solid and dashed curves are representing data with and without the subtraction of uncorrelated events, respectively. Visible peaks (solid curve) are strongly populated discrete states in  $^{74}\text{Ge}$ .  $S_n$  indicates the location of the neutron separation energy.

cation spectrum. A projection of  $\alpha - \gamma$  coincidences onto the  $\alpha$ -particle axis is shown in Fig. 1. The selection of correlated events was made with a coincidence time of less than 140 ns by placing appropriate gates around the prompt time peak. Uncorrelated event contributions were extracted and subtracted from the data by placing off-prompt time gates to the early and late sides of the prompt timing peak.

Kinematic corrections due to the recoil energy of  $^{74}\text{Ge}$  and the energy losses of scattered  $\alpha$ -particles in the target and aluminum foils were applied to the  $\alpha$ -particles. Although the target contained some oxygen and carbon contaminants, the recoil corrections for the scattered  $\alpha$ -particles from  $^{74}\text{Ge}$  are quite different compared to those of light contaminant nuclei, thereby allowing a clean extraction of the events of interest. For instance, the corrections from  $^{74}\text{Ge}$  versus  $^{16}\text{O}$  differ by  $\sim 1 \text{ MeV}$  and  $\sim 10 \text{ MeV}$  at  $20^\circ$  and  $72^\circ$  detection angles, respectively. The energy resolution of the  $\Delta E - E$  telescopes, measured from the elastic peak, was  $\approx 250 \text{ keV}$ . Despite the low velocities of the  $^{74}\text{Ge}$  recoils, corrections for Doppler effects of the high-energy  $\gamma$ -rays were found to be necessary and useful.

Transitions ( $E_\gamma$ ) to the ground state were extracted with the condition  $|E_\gamma - E_x| \leq 130 \text{ keV}$  imposed on the  $\alpha - \gamma$  coincidence events, where  $E_x$  refers to the excitation energy of the decaying state and is determined from the energy of the scattered  $\alpha$ -particles. Placing this stringent energy requirement upon the data, together with the differences in kinematic properties ensures that only transitions from  $^{74}\text{Ge}$  are extracted, eliminating contributions due to contaminants.

Additionally, various combination of angles between the direction of the recoiling nuclei (as defined by the  $\alpha$  particles detected in the particle telescope) and the  $\gamma$ -

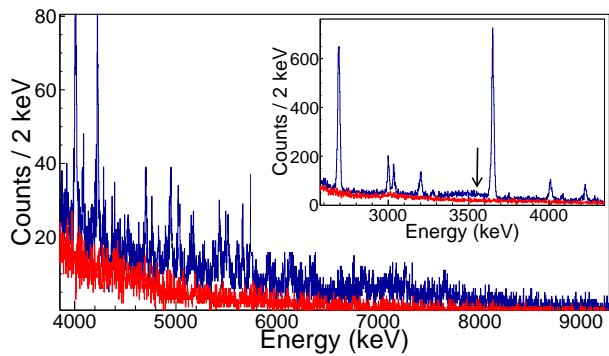


FIG. 2. (Color online) Spectrum of  $\gamma$ -ray transitions decaying directly to the ground state from defined excitation energies. Blue and red spectra correspond to correlated and uncorrelated events, respectively. Inset: the lower energy part of the spectrum where the arrow indicates the position of the unobserved 3558-keV transition, known from  $(\gamma, \gamma')$  experiments [39, 40].

rays detected in the Clover detectors were used for the determination of angular distributions.

#### IV. RESULTS AND DISCUSSION

The spectrum of direct  $\gamma$ -ray transitions to the ground state is shown in Fig. 2, where in addition to many states for  $E_x < 6$  MeV, a high concentration of states/strength is also observed for  $6.5 < E_x < 8$  MeV. Although the overall sensitivity to high-energy transitions is relatively poor, many transitions observed in  $(\gamma, \gamma')$  experiments [39, 40] can also be clearly identified in the present data. Unresolved strength was separated from intensities of individual transitions by simultaneously fitting the peaks using the ROOT analysis package [44] in a 16 keV per channel compressed  $\gamma$ -ray spectrum. The unresolved, underlying intensity for  $6.5 < E_x < 8$  MeV amounts to  $\approx 50\%$ . Comparisons with the recent  $(\gamma, \gamma')$  measurement [40] reveal several states, which were not populated in the  $(\alpha, \alpha'\gamma)$  reaction, but are observed in the  $(\gamma, \gamma')$  measurement. However, the states at  $E_x = 6850$  and  $7060$  keV are populated only through the  $(\alpha, \alpha'\gamma)$  reaction.

The multipole nature of the high-energy transitions was determined through angular distribution measurements, shown in Fig. 3. Because of the paucity of the data, the angular distribution was extracted simultaneously for the total (resolved and unresolved)  $\gamma$ -ray strength in the interval  $6.5 < E_x < 8$  MeV. For comparison, angular distributions of known dipole ( $E_\gamma = 2690$  keV and  $E_\gamma = 3648$  keV) and quadrupole transitions ( $E_\gamma = 596$  keV) in  $^{74}\text{Ge}$  are also included in Fig. 3. Although the  $6.5 < E_x < 8$  MeV strength does not exhibit a perfect agreement with the expected distribution of a dipole transition, the similarity to the two known dipole transitions strongly supports the overall dipole na-

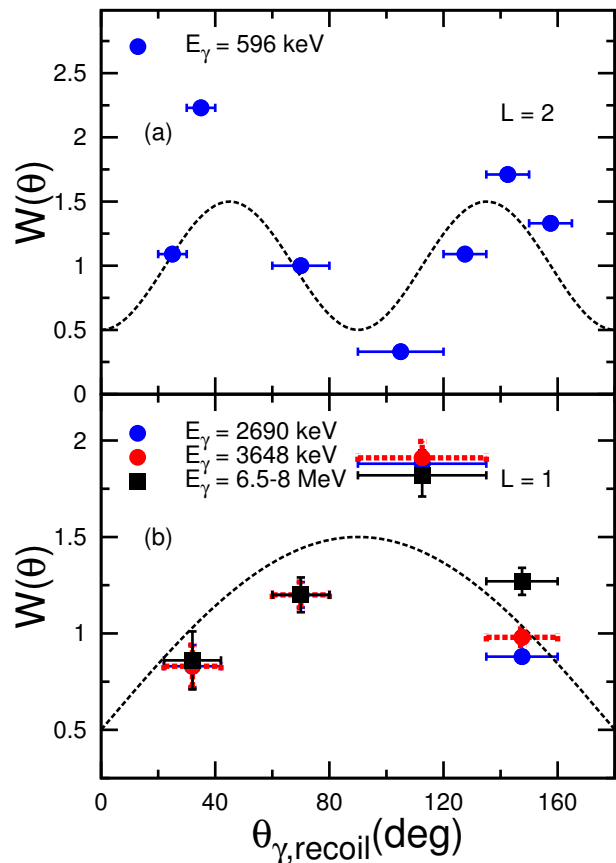


FIG. 3. (Color online) Angular distributions of (a) the first-excited state  $l = 2$  596-keV transition, and (b)  $l = 1$  transitions from the known 2690 and 3648 keV states together with the total strength of resolved and unresolved transitions for  $6.5 < E_x < 8$  MeV in  $^{74}\text{Ge}$ .

ture. Natural-parity states are preferentially populated in this reaction [45], leading to an assignment of spin-parity  $J^\pi = 1^-$  to the decaying states.

In Fig. 4 panel (a), relative cross-sections of observed  $J^\pi = 1^-$  states are plotted and normalized to the 4007 keV state. For comparison, panel (b) of Fig. 4 displays relative integrated scattering cross-sections ( $I_s$ ) from  $(\gamma, \gamma')$  data [40], where the 4007 keV state is taken as the reference once again. All states for  $E_x > 6$  MeV from the  $(\gamma, \gamma')$  data are assumed to have negative parity and are plotted in Fig. 4, whereas in both panels only states have been included with known negative parity for  $E_x < 6$  MeV, as deduced from the  $(\gamma, \gamma')$  data. An exception are the states 2690, 3033, and 3648 keV with assigned  $J^\pi = 1, 1, 1^+$ , respectively [39]. The  $J^\pi = 1^+$  assignment to the 3648 keV state is based on a polarization measurement [39]. However, this state has also been observed in an earlier  $(\alpha, \alpha')$  work [46]. Since inelastic  $\alpha$ -scattering populates preferentially natural-parity states, the observed strong cross section in the present experiment contradicts this assignment. Hence, the transition is assumed to be electric dipole in character. Similar considerations are applied to the 2690 and 3033 keV states.

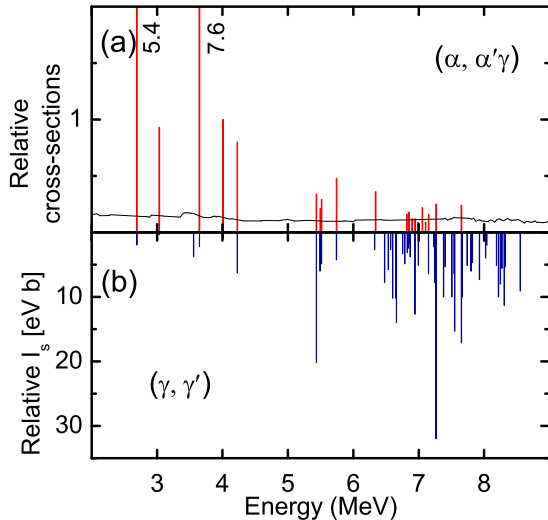


FIG. 4. (Color online) In panel (a) relative cross-sections of  $E1$  transitions from the  $(\alpha, \alpha'\gamma)$  data are plotted, while in panel (b) the relative integrated scattering cross-sections  $I_s$  obtained from  $(\gamma, \gamma')$  data [40] are shown. Numbers next to some transitions indicate the total value of relative cross section. In panel (a), the sensitivity limit is shown by the black solid curve and was determined using the procedure outlined in Ref. [11]. Uncertainties on the cross-sections in panel (a) are  $\sim 50\%$  for weakly populated states and decrease to  $\sim 15\%$  for strongly populated states.

The complete absence of the 3558 keV state in the present data (see arrow in inset of Fig. 2) is noteworthy, since this state has been observed in the  $(\gamma, \gamma')$  work and was assigned  $J^\pi = 1^{(-)}$  [39].

The comparison shows the presence of two different regions in the energy range of the investigated dipole excitations. In the lower part ( $3 < E_x < 6$  MeV) the excitations due to  $(\alpha, \alpha'\gamma)$  are enhanced compared to the upper part ( $6 < E_x < 9$  MeV). For  $(\gamma, \gamma')$  excitations the trend is reversed indicating a dominant isovector nature of the higher-energy dipole excitations. This reduction in relative cross-section in the  $(\alpha, \alpha'\gamma)$  data becomes even more pronounced if the intensity of the 3648-keV state is taken as a normalization reference.

The reduction of cross-sections in the  $(\alpha, \alpha'\gamma)$  data for states  $E_x > 6$  MeV, compared to cross-sections for  $E_x < 6$  MeV, is larger than observed in previous cases. Indeed, with respect to  $(\alpha, \alpha'\gamma)$  studies on  $^{140}\text{Ce}$ ,  $^{138}\text{Ba}$  and  $^{124}\text{Sn}$  [10, 11, 13], the isoscalar response at low energies ( $< 6$  MeV) is much stronger. The current result shows that many of the dipole excitations in the  $6 < E_x < 9$  MeV range in  $^{74}\text{Ge}$  are mixed with larger isovector components. However, a few weakly populated pure isoscalar, as well as several pure isovector states are found for  $E_x > 6$  MeV. These results indicate that the dipole excitations in  $^{74}\text{Ge}$  for  $E_x > 6$  MeV do show the

common scenario of dipole excitations splitting in two distinct parts: one at lower energy, whose states have a strong isospin mixing, and one at higher energy with predominant isovector character.

We have performed calculations of the dipole transition densities in  $^{74}\text{Ge}$  within the Relativistic Quasiparticle Time Blocking Approximation (RQTBA) [47] based on the covariant energy density functional theory (CEDFT) [48, 49]. The RQTBA has been developed to include spreading mechanisms, other than Landau damping (one particle - one hole (1p1h), or two-quasiparticle (2q), configurations) into the microscopic description of nuclear excitation modes within the relativistic framework. The existing versions of RQTBA include  $2q \otimes$  phonon [47] or two phonon [50, 51] configurations in a fully self-consistent way. Parameters (in the present version with the NL3\* [52] interaction - 8 parameters) of the CEDFT were fixed by fitting masses and radii of several characteristic nuclei throughout the nuclear chart [49] and no adjustments were involved in the subsequent calculations.

The calculations were performed in the following three steps: (i) the single-particle spectrum was obtained from the self-consistent relativistic mean-field solution; (ii) the phonon spectrum was computed by the self-consistent relativistic quasiparticle random phase approximation (RQRPA) and (iii) the Bethe-Salpeter equation for the nuclear dipole response was solved within the RQTBA employing the RQRPA phonons to construct the induced energy-dependent residual interaction. The low-energy region of the dipole spectrum is calculated with the RQTBA. It includes mixing of quasiparticles with phonons, in particular, with the lowest  $2^+$  collective state obtained in CEDFT at  $E_x \sim 0.6$  MeV and the lowest  $3^-$  state at  $E_x \sim 3.4$  MeV, while without mixing there is no dipole strength at these energies. The phonon spectra are consistent with experimental observations for the first-excited  $2^+$  and  $3^-$  states at 596 and 2536 keV [53]. Reduced transition probabilities from RQTBA calculations with 25 keV smearing (bunching) for isoscalar and isovector dipole operators are plotted in panels (a) and (b) of Fig. 5. Although these calculations also suggest a suppression in the isoscalar  $E1$  strength at higher energies, they underestimate the experimentally observed suppression in  $^{74}\text{Ge}$ .

Figure 6 shows the proton, neutron, isoscalar and isovector transition densities for calculated states at  $E_x = 4.55$  and 7.05 MeV. The lower-lying state (panel (a)) exhibits the usual pattern for an almost pure isoscalar dipole state, with the proton and neutron transition densities in phase inside the nucleus and at the nuclear surface. Consequently, the isoscalar transition density has a pattern typical of the compressional mode with a node close to the nuclear surface. In contrast, the higher-lying state (panel (b)) exhibits the typical behavior of a Pygmy dipole state where the proton and neutron transition densities are in phase inside the nucleus, while at the surface region the contribution comes from the neutron density only. Consequently, at the surface the

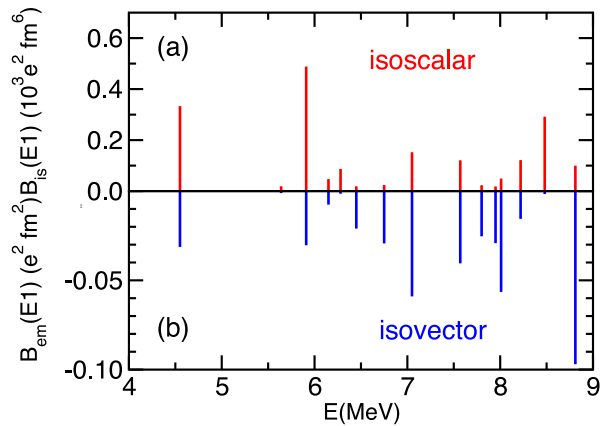


FIG. 5. (Color online) Reduced transition probabilities in  $^{74}\text{Ge}$  from RQTBA calculations plotted for the isoscalar (a) and electromagnetic (isovector) (b) dipole operators.

isoscalar and isovector transition densities have the same intensity giving rise to a strong isospin mixing. For the calculated dipole states this behavior is supported by the present data, which manifests significant isospin mixing in the energy region under investigation.

An estimate of the inelastic cross section of states due to different reaction mechanisms is obtained using the TALYS 1.6 reaction code [54]. These calculations suggest that for a 48 MeV  $\alpha$  beam, the compound reaction does not contribute at any excitation energy under consideration, while for  $E_x \approx 6$  MeV the contribution from pre-equilibrium reactions is an order of magnitude less than that from direct reactions and gradually increases with  $E_x$ . Therefore, a direct comparison with other experimental data should be taken with some degree of caution at the highest excitation energies.

In principle, the presence of the Coulomb interaction between the target and projectile has the capability to substantially contribute to the observed cross-sections [55]. To investigate the effect of the Coulomb interaction on the observed inelastic cross sections, theoretical cross sections were calculated both with and without taking the Coulomb interaction into account. These theoretical

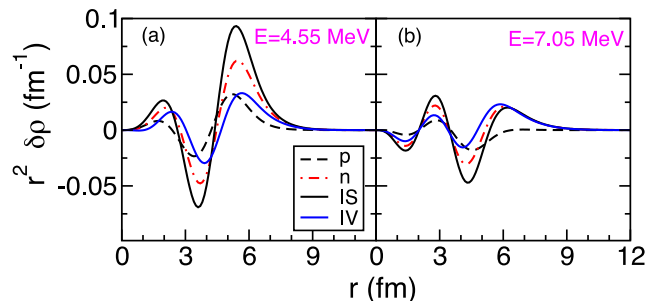


FIG. 6. (Color online) Transition densities for two calculated RQTBA states at  $E_x=4.55$  (panel (a)) and 7.05 MeV (panel (b)) in  $^{74}\text{Ge}$ .

cross sections were obtained for the dipole states at  $E_x = 4.55$  and 7.05 MeV by performing Distorted Wave Born Approximation (DWBA) calculations, carried out using the FRESKO code [56]. The radial nuclear form factors were constructed within a double folding procedure using the microscopic transition densities of Fig. 6, see Ref. [57] for more details on the procedure. For the Coulomb form factors we have used the analytic expression built inside the FRESKO code. For these calculations the double folding potential was used as the real part of the optical potential, while for the imaginary part the same geometry as for the real part but with half the intensity was chosen [57]. These results are shown in Fig. 7 where a negligible difference between the calculations performed using only the nuclear interaction (red curve) and using both the nuclear and Coulomb interaction (blue curve) is observed for the detection angles under study (blue shaded areas). For these low-lying dipole states it has been shown that the nuclear and Coulomb contributions interfere constructively in the nuclear surface region [55]. This feature is expected not to be visible for this relatively low incident energy since the Coulomb contribution becomes important as the beam energy increases towards 30 MeV/u [55, 58]. We are aware of the fact that, while the relation between the inelastic cross section and the  $B_{em}(E1)$  is clear for the Coulomb excitation (they are proportional), the relation between the isoscalar response and the inelastic excitation cross section due to an isoscalar probe is not so evident. In fact, the ratio between the  $B_{is}(E1)$  of the two states at 4.55 and 7.05 MeV is 2.2 while the ratio between the corresponding values of the cross sections is 6.4 at the first maximum. If we eliminate the effect of the Q-value, by placing the two states at the same energy, then the ratio decreases to 4.1, still far from 2.2. However, in Ref. [55] a calculation

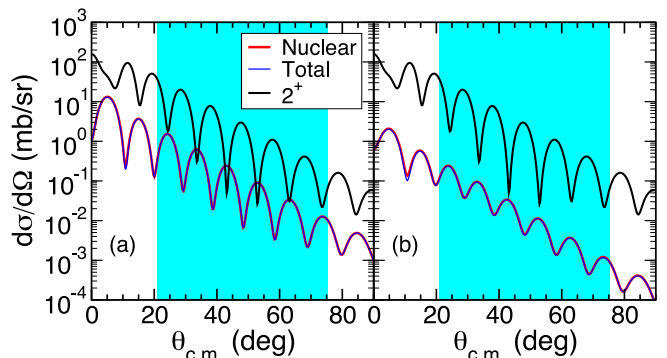


FIG. 7. (Color online) Cross sections of inelastic scattering of  $\alpha$ -particles are plotted as a function of scattering angle in the center of mass frame for the  $2^+$  state in  $^{74}\text{Ge}$  at 596 keV and dipole states at (a) 4.55 and (b) 7.05 MeV. The blue shaded areas represent the angular coverage of scattered  $\alpha$ -particles in the present measurement.

of the cross section was presented in the framework of a semiclassical model, that provides the missing link to directly compare the results from the microscopic RQTBA calculations to experimental data measured via the ( $\alpha$ ,  $\alpha'\gamma$ ) reaction, confirming the structural splitting of the low-lying  $E1$  strength.

It is instructive to also have an estimate of the cross-section of states with higher multiplicities. Therefore, we also performed calculations for the first-excited  $2^+$  state in  $^{74}\text{Ge}$ , using a collective macroscopic nuclear form factor. The  $B(E2)$  value of the 596 keV transition is taken to be  $3050 e^2 fm^4$  from Ref. [59] with a deformation length of 1.43 fm. The results are shown in Fig. 7, where the cross-sections for the  $2^+$  state (black curve) are significantly higher when compared to the dipole states. This is not only the case for the detection angles of the present experiment, but also for very forward angles.

It is interesting to point to a recent measurement of the photon strength function below the neutron separation energy in  $^{74}\text{Ge}$  [60], using the so-called Oslo Method. Despite the limited  $\gamma$ -ray detection resolution, a broad structure is observed in the  $6 < E_\gamma < 8$  MeV range. It is highly probable that this feature is the same Pygmy dipole resonance structure as observed in this work.

## V. SUMMARY AND CONCLUSION

We provide new results, which indicate a suppression in relative cross section for the excitation of the PDR

in  $^{74}\text{Ge}$  populated through inelastic  $\alpha$ -scattering, when compared to photon scattering data for  $E_x > 6$  MeV. The observed dipole response splits into two distinct parts: one at lower energy, with excitations that have strong isospin mixing, and one at higher energy with predominant isovector character. The results are particularly important in improving our understanding of the emergence and persistence of the PDR for low  $N/Z$  nuclei. As such, measurements in other mass regions are undoubtedly necessary to fully understand the evolution of the PDR from near-isospin saturated systems towards nuclei with large  $N/Z$  ratios. Finally, the present work highlights the importance of using complementary probes to photon scattering, in order to reveal detailed information about the underlying nature of dipole excitations.

## VI. ACKNOWLEDGMENTS

The authors would like to thank the operational staff at iThemba LABS for providing excellent beam quality throughout the experiment and Lawrence Berkeley National Laboratory for making available the  $^{74}\text{Ge}$  target. This work was supported by the National Research Foundation of South Africa under grant no. 92789, by the Research Council of Norway, project grant nos. 205528, 213442, and 210007, by US-NSF grants PHY-1204486 and PHY-1404343 and the US Department of Energy under contract no. DE-AC52-07NA27344.

- 
- [1] N. Paar, D. Vretenar, E. Khan, and G. Colò, Rep. Prog. Phys. **70**, 691 (2007).
  - [2] D. Savran, T. Aumann, and A. Zilges, Prog. Part. Nucl. Phys. **70**, 210 (2013).
  - [3] A. Bracco, F. C. L. Crespi and E. G. Lanza, Eur. Phys. J. A **51**, 99 (2015).
  - [4] A. M. Lane, Ann. Phys. **63**, 171 (1971).
  - [5] P. -G. Reinhard and W. Nazarewicz, Phys. Rev. C **87**, 014324 (2013).
  - [6] L. Pellegrini *et al.*, Phys. Lett. B **738**, 519 (2014).
  - [7] F. C. L. Crespi *et al.*, Phys. Rev. C **91**, 024323 (2015).
  - [8] I. Poltoratska *et al.*, Phys. Rev. C **85**, 041304(R) (2012).
  - [9] A. M. Krumbholz *et al.*, Phys. Lett. B **744**, 7 (2015).
  - [10] D. Savran *et al.*, Phys. Rev. Lett. **97**, 172502 (2006).
  - [11] J. Endres, *et al.*, Phys. Rev. C **80**, 034302 (2009).
  - [12] T. D. Poelheken *et al.*, Phys. Lett. B **278**, 423 (1992).
  - [13] J. Endres, *et al.*, Phys. Rev. Lett. **105**, 212503 (2010).
  - [14] V. Derya *et al.*, J. Phy. Conf. Ser. **366**, 012012 (2012).
  - [15] V. Derya *et al.*, Nucl. Phys. **A906**, 94 (2013).
  - [16] V. Derya *et al.*, Phys. Lett. B **730**, 288 (2014).
  - [17] F. C. L. Crespi *et al.*, Phys. Rev. Lett. **113**, 012501 (2014).
  - [18] S. Volz *et al.*, Nucl. Phys. **A779**, 1 (2006).
  - [19] K. Govaert *et al.*, Phys. Rev. C **57**, 2229 (1998).
  - [20] C. Romig *et al.*, Phys. Rev. C **88**, 044331 (2013).
  - [21] T. Shizuma *et al.*, Phys. Rev. C **78**, 061303 (2008).
  - [22] R. Schwengner *et al.*, Phys. Rev. C **76**, 034321 (2007).
  - [23] N. Benouaret *et al.*, Phys. Rev. C **79**, 014303 (2009).
  - [24] A. Makinaga *et al.*, Phys. Rev. C **82**, 024314 (2010).
  - [25] N. Tsoneva, and H. Lenske, Phys. Rev. C **77**, 024321 (2008).
  - [26] N. Paar *et al.*, Phys. Rev. Lett. **103**, 032502 (2009).
  - [27] M. Martini, S. Péru, and M. Dupuis, Phys. Rev. C **83**, 034309 (2011).
  - [28] M. Tohyama, and T. Nakatsukasa, Phys. Rev. C **85**, 031302(R) (2012).
  - [29] D. Vretenar *et al.*, Phys. Rev. C **85**, 044317 (2012).
  - [30] H. Nakada, T. Inakura, and H. Sawai, Phys. Rev. C **87**, 034302 (2013).
  - [31] S. Goriely, Phys. Lett. B **436**, 10 (1998).
  - [32] S. Goriely, E. Khan, and M. Samyn, Nucl. Phys. **A739**, 331 (2004).
  - [33] E. Litvinova *et al.*, Nucl. Phys. **A823**, 26, (2009).
  - [34] I. Daoutidis, and S. Goriely, Phys. Rev. C **86**, 034328 (2012).
  - [35] J. Piekarewicz, Phys. Rev. C **73**, 044325 (2006).
  - [36] J. Piekarewicz, Phys. Rev. C **83**, 034319 (2011).
  - [37] L. Rosier, and E. I. Obiajunwa, Nucl. Phys. A **500**, 323 (1989).
  - [38] P. Möller *et al.*, At. Data Nucl. Data Tables **94**, 758 (2008).
  - [39] A. Jung *et al.*, Nucl. Phys. **A584**, 103 (1995).

- [40] R. Massarczyk *et al.*, Phys. Rev. C **92**, 044309 (2015).
- [41] M. Lipoglavšek *et al.*, Nucl. Instr. Meth. Phys. Res. A **557**, 523 (2007).
- [42] <http://www.micronsemiconductor.co.uk/pdf/w1.pdf>
- [43] <http://www.xia.com>
- [44] <https://root.cern.ch>
- [45] W. W. Eidson and J. G. Cramer, Jr., Phys. Rev. Lett. **9**, 497 (1962).
- [46] B. Schürmann *et al.*, Nucl. Phys. **A475**, 361 (1987).
- [47] E. Litvinova, P. Ring, and V. Tselyaev, Phys. Rev. C **78**, 014312 (2008).
- [48] P. Ring, Prog. Part. Nucl. Phys. **37**, 193 (1996).
- [49] D. Vretenar *et al.*, Phys. Rep. **409**, 101 (2005).
- [50] E. Litvinova, P. Ring, and V. Tselyaev, Phys. Rev. Lett. **105**, 022502 (2010).
- [51] E. Litvinova, P. Ring, and V. Tselyaev, Phys. Rev. C **88**, 044320 (2013).
- [52] G. A. Lalazissis *et al.*, Phys. Lett. B **671**, 36 (2009).
- [53] <http://www.nndc.bnl.gov> (as of April 2015).
- [54] A. J. Koning *et al.*, *Nuclear Data for Science and Technology* (EDP Sciences; eds O. Bersillon *et al.*), p. 211 (2008) (see also <http://www.talys.eu>).
- [55] E. G. Lanza *et al.*, Phys. Rev. C **89**, 041601(R) (2014).
- [56] I. J. Thompson, Comp. Phys. Rep. **7**, 167 (1988); <http://www.fresco.org.uk>
- [57] E. G. Lanza, A. Vitturi, and M. V. Andrés, Phys. Rev. C **91**, 054607 (2015).
- [58] E. G. Lanza *et al.*, Phys. Rev. C **84**, 064602 (2011).
- [59] R. Leconte *et al.*, Phys. Rev. C **22**, 2420 (1980).
- [60] T. Renstrøm *et al.*, Phys. Rev. C **93**, 064302 (2016).